Digest Journal of Nanomaterials and Biostructures Vol. 19, No. 4, October-December 2024, p. 1617-1632

SnO_2 and $Sn_{0.95}M_{0.05}O_2$ [M=Fe, Co and Cu] thin films: synthesis, characterization and photocatalytic activity

S. Roguai[a,*], A. Lakel[b], A. Djelloul[c]
[a,c]*LASPI2A Laboratory of Structures, Properties and Interatomic Interactions, Abbes Laghrour University, Khenchela 40000, Algeria*
[a,c]*Science of Matter, Abbes Laghrour University, Khenchela 40000, Algeria*
[b]*Laboratory of Metallic and Semiconducting Materials, University of Biskra, BP 145 RP, 07000 Biskra, Algeria*

On discussed the relationship between the nature of dopant (Cu, Co, Fe)-SnO_2 and their structural, morphological, optical, electrical, and photocatalysts characteristics. We prepared the films on glass substrates using the spray pyrolysis technique. Detailed analysis by X-ray diffraction (XRD) revealed that all obtained thin films crystallized in a rutile tetragonal structure. A homogeneous and compact surface with an important dimension of grains was revealed by observation (SEM) for the doped films. The transmittance spectra results indicated that the layers are dependent on the doping nature and that the doping leads to a broadening of the calculated bandgap. Lastly, the Seebeck coefficient rises from │76│for undoped SnO_2 to │110│for Co-doping, │133│for Cu-doping, and declines with Fe- doping (│71│µV/K). While the concentration of carriers decreases by 1.96×10^{19}, 9.80×10^{18}, and 6. 66×10^{18} cm-³ for SnO_2, $Sn_{0.95}Co_{0.05}O_2$, and $Sn_{0.95}$ $Cu_{0.05}O_2$ thin films, respectively, and increased for Fe doping (6.17×10^{19} cm-³). These electrical properties indicated that the resistivity is affected by the nature of the doping. For the photocatalytic tests, the best performance was observed for samples $Sn_{0.90}Fe_{0.05}$ O_2 (45% rate of degradation).

(Received August 13, 2023; Accepted October 24, 2024)

Keywords: (Co, Fe, Cu)-doped SnO_2 Thin films, Spray pyrolysis, Seebeck coefficient, Optical properties

1. Introduction

Transparent and conductive oxides (OTCs) in thin films such as SnO_2, ZnO, TiO_2, CuO, etc, are important materials to play dual property, electrical conductivity and transparency in the visible [1]. Studies on transparent oxide semiconductors with high electrical conductivity have attracted the attention of many researchers because of their various applications in the optoelectronics industry[1]

Tin oxide (SnO_2), is an important and useful semiconductor that has good transparency and electrical conductivity in the visible range and has a large bandgap energy value varying between 3.6 and 4 eV[2-4]. The electronic band structure of SnO_2 is necessary to understand its electro-optical properties. The electronic configurations of Sn^{4+} and O^{2-}, knowing that the atomic numbers of Sn and O will be 50 and 8 respectively, are as follows:

Sn4+:$1s^2$ $2s^2$ $2p^6$ $3s^2$ $3p^6$ $4s^2$ $3d^{10}$ $4p^6$ $4d^{10}$ ($5s^05p^0$...). O2- : $1s^2$ $2s^2$ $2p^6$ ($3s^0$...). One can see that the completely ionic model describes the position of the energy levels in the crystal, finds a direct band gap of the order of of the order of 5 eV (experimental values between: 3.5 and 4 eV at 20°C). The highest level of the valence band is a p state of oxygen and the lowest level of the conduction band is an s state of oxygen. Conduction band is an s state of tin. The last core levels are the Sn $4d_{5/2}$ and Sn $4d_{3/2}$ states which are located at 22.2 eV and 23.2 eV respectively[5]. All these properties make SnO2 a suitable material for technological applications like solar cells and energy storage, photo-catalysis, gas sensors, conductive transparent electrodes and opto-electronic technologies [6,7].

* Corresponding author: rog.sabrina@yahoo.fr
https://doi.org/10.15251/DJNB.2024.194.1617

The doping of tin oxide with transition metals (TM) (Fe, Cu, Co, Ni, etc.) is more studied due to their electronic, optical properties and remarkable magnetic values due to the presence of strong sp - d exchange interactions at the magnetic ions and band electrons [8], another point of great interest for the properties of SnO_2 is its ferromagnetic behavior at room temperature. To improve these properties, many research groups have doped tin oxide with transition metal ions such as Ca, Al, Co, Fe, Zn, Mn, Ni, Cu, and Sb [9, 10], which leads to an enhancement of its optical, magnetic and electronic properties[11].

The doping of SnO_2 with the Iva group (Fe, Co, and Cu) has attracted a lot of interest recently as a candidate for dilute magnetic semiconductor (DMS) materials, for doping with Cobalt and copper play a very important role to emanate ferromagnetism in SnO_2 and makes it suitable for spintronic devices[12,13]. As well as doping with Fe has the advantage of a lower surface potential barrier than that of metals and high catalytic activity, which can be very vital in the field of electron emission [14]. Previously studies show that doping with the transition metals cobalt and iron at a doping rate of 4%, affects the transmittance of the films, with large grain area compared to pure films, as well as the resistivities decreased with doping [15]

To synthesize pure and doped SnO_2 thin films, several methods have been developed and reported in the literature. Such as pulsed laser deposition [16], thermal evaporation [17], sputtering [18], co-precipitation [19], spray pyrolysis, and sol-gel deposition [20]. Among these techniques, we are using the spray pyrolysis technique, because of its simplicity and low cost of the equipment, the large homogeneous surface, and the easy control of the structure of the deposited films [21].

In this search, we found the effect of the doping with group VIIIA (Fe, Co, and Cu) 5at.%, on the structural, microstructural, optical, and electrical properties of SnO_2, and its photocatalytic activity are discussed. This percentage (5 at.%) is selected due to the fact that it represents the solubility limit of these elements for the SnO_2 doping.

2. Experimental part

2.1. Film preparation

Thin films of SnO_2, $Sn_{0.90}M_{0.05}O_2$ [M = Fe, Co, and Cu] were grown using the spray pyrolysis route. The composition of the solutions employed in the deposition is as follows: 0.01 M tin chloride [$SnCl_4$, $2H_2O$] (Fulka 99.9%) and copper chloride ($CuCl_2 \cdot 2H_2O$) (Fulka 99.9%) (5) (Cu, at%), cobalt nitrate hexahydrate [Co $(NO_3)_2 \cdot 6H_2O$] (Fulka 99.9%) (5) (Co, at%), ferric chloride ($FeCl_3$) (Fulka 99.9%) (5) (Fe, at%) as precursors dopant source Cu, Co, and Fe respectively. Where dissolved the tin chloride [$SnCl_4$, $2H_2O$] (0.01M) in 1.2 ml HCl (Merck 99.5%) was stirred vigorously for 10 min at 80 °C. After stirring, the various dopants (Fe, Co, and Cu) were added to the solution for the preparation of these chlorides with a concentration equal to 5 at. %. To the solution, it was added 10 ml of CH_3OH (Merck 99.5%) and 7 ml of deionized water, and then the solution was vigorously mixed for 30 min. Before the deposition process, the glass substrate was cleaned with acetone and hydrochloric acid, rinsed with deionized water, and dried in the air, more details about the deposition can be found in the paper [22,23]. Lastly, the pure and doped films were deposited on the glass substrates heated to 450°C

2.2. Photocatalytic activity

The photocatalytic activity of undoped and $Sn_{0.95}M_{0.05}O_2$[M=Fe, Cu and Co] thin films were studied via the degradation of a methylene blue solution (10 ml) under exposure to UV light at room temperature. The UV source used was a Philips germicidal lamp (G15T8/15 W). The photocatalytic degradation process was evaluated by measuring the absorbance of the MB solution every 30 minutes for 300 minutes using a UV-vis spectrophotometer (SpectroScan 80D). The degradation rate of MB is calculated using the following formula:

$$Degradation\ rate(\%) = \frac{C_0 - C_t}{C_0} \times 100 = \frac{A_0 - A_t}{A_0} \times 100 \quad (1)$$

where C_0 is the initial concentration, C_t is the concentration after 't' min. A is the initial absorbance and A_t is the absorbance after 't' min.

2.3. Characterization techniques

SnO_2, $Sn_{0.90}M_{0.05}O_2$ [M = Fe, Co, and Cu] thin films were analyzed by XRD, SEM, FTIR, and the optical absorption and photoluminescence properties were studied in detail. The structural properties were recorded using a PANalytical Empyrean diffractometer equipped with Cu-Kα radiation (λ= 1.5418 Å). The thin film surface observations were characterized using scanning electron microscopy (SEM) (a JEOL JSM 7500F microscope). To evaluate the optical properties of the thin films, a Perkin Elmer UV-VIS-NIR Lambda 19 spectrophotometer was used in the 190-1800 nm spectral range. Thermo-Nicolet equipment was used to monitor the FTIR spectra in the 4000-400 cm^{-1} region. The Seebeck coefficient was determined based on the detected Seebeck voltage and the temperature difference from 0 K to 200 K with an increment of 20 K.

3. Results and discussion

3.1. Structural analysis

The analyses of XRD spectra of SnO_2, $Sn_{0.90}M_{0.05}O_2$ [M = Fe, Co, and Cu] thin films are displayed in Figure a.1. We notice that all peaks correspond to the tetragonal rutile structure of SnO2 with JCPDS map number (77-0452, space group P42 / mnm)). And that by the peaks (110), (101), (200), (211), (310), (301), and (321), which correspond to the angle 2θ around 2θ: 26.61°, 33.92°, 38.06°, 51.68°, 61.86°, 65.80°, and 81.22° respectively [24], with varying intensities. Also, it is noticed that there is no trace of an impurity phase peak from the dopants (Fe, Co, and Cu) such as Fe_2O_3, Fe_3O_4, CoO, and CuO, respectively [8]. This indicates that (Fe, Co, and Cu) are well incorporated in the SnO_2 lattice.

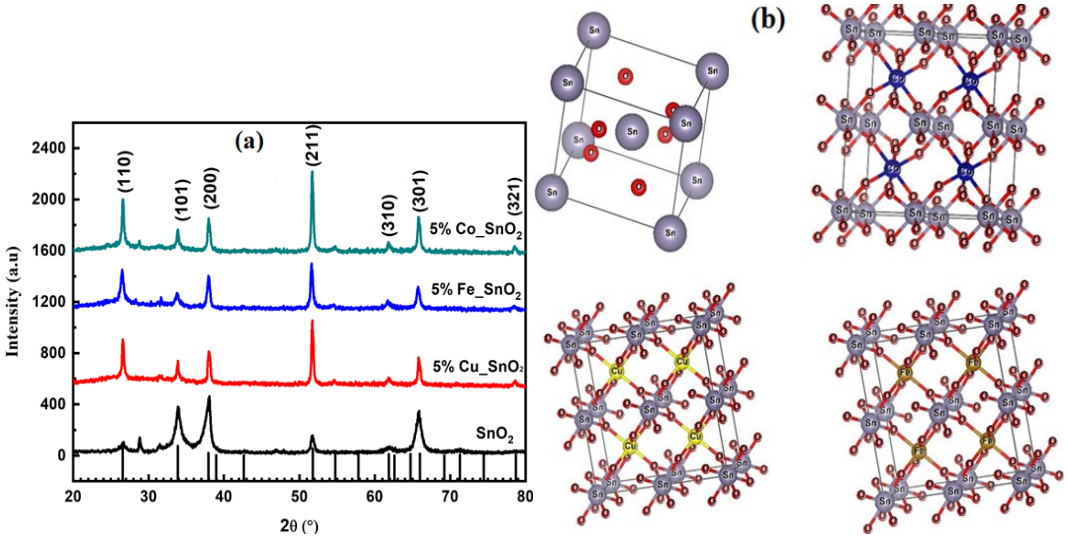

Fig. 1. a) XRD patterns of SnO_2, $Sn_{0.95}M_{0.05}O_2$[M = Fe ,Co, and Cu] sprayed thin films; b) SnO_2 and (Co, Cu and Fe)-SnO_2 crystal structure.

The XRD spectra show that the (200) peak is more intense than the others, for the SnO_2 thin films, which suggests that (200) is the preferential direction. For the case of doping confused with the (211) peak. This displacement towards (211) corresponds to the interaction produced between the incorporated Fe, Co, and Cu metal ions and those of the SnO_2 lattice. This explains the improvement of the crystalline properties of the doped films compared to those of pure SnO_2 [25].

It can be seen from figure a.1, a slight shift of the peak to lower angles is observed for pure SnO_2 films (26.62°) compared to doped films (SnO_2/Fe, SnO_2/Co and SnO_2/Cu) with a shift of 26.53°, 26.61° and 26.54° respectively), in proportion with the width at half height, so we can assume that the dopant ion in our thin films is primarily in the 2+ state. However, some amount of 3+ states cannot be neglected. It is well known that a difference in the ionic radii of Fe^{+2} (0.77 A°), Co^{+2} (0.72 A°), Cu^{+2} (0.73 A°) and Sn^{+4} (0.69 A°) causes an increase in the lattice. Therefore, the shift to lower angles can be attributed to a change in the lattice parameters with a rise in the grain size of the doped thin films [26]

The lattice constants (a) and (c) of Sn0.95M0.05O2 [M= Fe, Co and Cu] films have been calculated according to the formula [27]:

$$\frac{1}{d_{hkl}^2} = \frac{(h^2+k^2)}{a^2} + \frac{l^2}{c^2} \quad (2)$$

The variation of the lattice parameters is presented in table 1. And it was found that there is an increment in the lattice constants with the doping (Co, Cu and Fe). This is probably due to the replacement of Sn^{4+} (0.69 A˚) ion by Fe^{2+} (0.77 A˚), Co^{2+} (0.72 A˚) and Cu^{2+} (0.73 Å) ions.

Table 1. Structural parameters of pure and 5%-(Co, Fe, Cu)-doped SnO_2 thin films.

Sample	**Plan (hkl)**	**$2\theta_{hkl}$ (deg.)**	**d spacing (Å)**	**B (deg.)**	**Lattice Constants (Å)**		**D (nm)**	**ε (%)**
					a	**c**		
SnO_2	(110) (101) (200) (211)	26.62 33.92 38.06 51.68	3.349 2.642 2.364 2.768	3.542 3.542 2.952 4.133	4.7364	3.1830	27.62	0.443
$Sn_{0.95}Fe_{0.05}O_2$	(110) (101) (200) (211)	26.53 33.81 38.04 51.58	3.359 2.650 2.365 1.771	2.362 2.952 2.362 2.066	4.7513	3.1937	41.29	0.270
$Sn_{0.95}Co_{0.05}O_2$	(110) (101) (200) (211)	26.61 33.89 37.94 51.66	3.349 2.645 2.371 1.769	1.771 2.066 2.066 1.771	4.7363	3.1885	52.92	0.242
$Sn_{0.95}Cu_{0.05}O_2$	(110) (101) (200) (211)	26.54 33.85 37.87 51.66	3.357 2.647 2.375 1.769	1.771 2.362 2.362 2.066	4.7483	3.1893	47.28	0.320

The diffractograms obtained in the θ-2θ range can be used to estimate the crystallite size in the thin film using the method of Debye and Scherrer, following the relation [28]:

$$D = \frac{0.9\lambda}{\beta \cos(\theta)} \quad (3)$$

where D: (in nm) average crystallite size in the direction perpendicular to the planes (hkl). k: constant, and its value is 0.89. λ: monochromatic wavelength of incident XRD. The value corresponds to the emission $K\alpha 1$ du copper: λ=0.1540598 nm. β: full width at half maximum (FWHM). θ: Bragg angle (in degrees) corresponding to the maximum of the diffraction peak. The results obtained are shown in Table.1, noting a strong increase in crystallite size with the nature of dopant at values of 41, 47, and 52nm for Fe-SnO_2, Cu-SnO_2, and Co-SnO_2 respectively, compared to undoped SnO_2 (27 nm). This behavior may be due to structural enhancement.

An inadequate microstress -strain- (ε) is one of the most important factors negatively influencing the structural properties resulting from a geometric mismatch at the interphase

boundaries between the film and substrate crystal lattices. The strain (ε) values of our films were calculated using the following formula [29]:

$$\varepsilon = \frac{\beta}{4\tan(\theta)} \quad (4)$$

From the results of Table 1, we can see that the deformation has an inverse variation to that of the size of the crystallites or as much there is an increase in the size of the crystallites, thus an improvement of the crystalline quality, as much there will be a decrease of the stresses which depend strongly on the deformation, and which is due to the decrease of the joints of grains and conversely.

Figure b.1 shows the structure of SnO_2, $Sn_{0.90}M_{0.05}O_2$ [M = Fe, Co, and Cu] thin films. The elemental lattice is generally tetragonal routile (a = b = 0.473 nm and c = 0.318 nm) and contains six atoms: two tin atoms and four oxygen atoms. In this case, each cation is the center of an almost regular octahedron formed by six oxygen atoms, while each oxygen atom is surrounded by three atoms of the cations located at the vertices of an isosceles triangle. The oxygen is in position 4f (space group P42/mmm) given by (u; u; 0), (1-u; 1-u; 0), (1/2+u; 1/2-u; 1/2) and (1/2-u; 1/2+u; 1/2) with u = 0.31. The cations are located: (1/2; 1/2; 1/2) and (0; 0; 0).

This tetragonal structure can be deformed and take the form of a pseudo tetragonal crystal or also called distorted tetragonal structure: it is therefore non-ideal. In the non-ideal structure, there is a different displacement of the positive charges (carried by the cations) and/or negative charges (carried by the anions) in the elementary mesh of the crystal. This can be caused by a particular orientation of the octahedra or by other phenomena such as oxygen vacancies or partial substitution of the Sn^{4+} cation by doping generating a partial cationic order of Sn^{4+}. In this structure, the barycenters of the charges are no longer confused.

3.2. Morphological characterization

Fig.2 shows SEM images of the c)SnO_2, a)5%Co-SnO_2, b)5%Cu-SnO_2, and d)5%Fe-SnO_2 films. As can be seen, these SEM images show that the surface of the developed films is uniform covering the entire film substrate without any defects or cracks, where the undoped SnO_2 sample (c) is smaller than that of doped SnO2 samples. This indicates that uniform nucleation occurred on the substrate surface during the development of the pure tin oxide films with (200) plane which confirms the results of XRD analysis. This shows a considerable improvement in the crystallographic characteristics of the film. We can also notice the significant change in the shape and size of the grains which is mainly due to the influence of the nature of the dopants (Fe, Co and Cu).

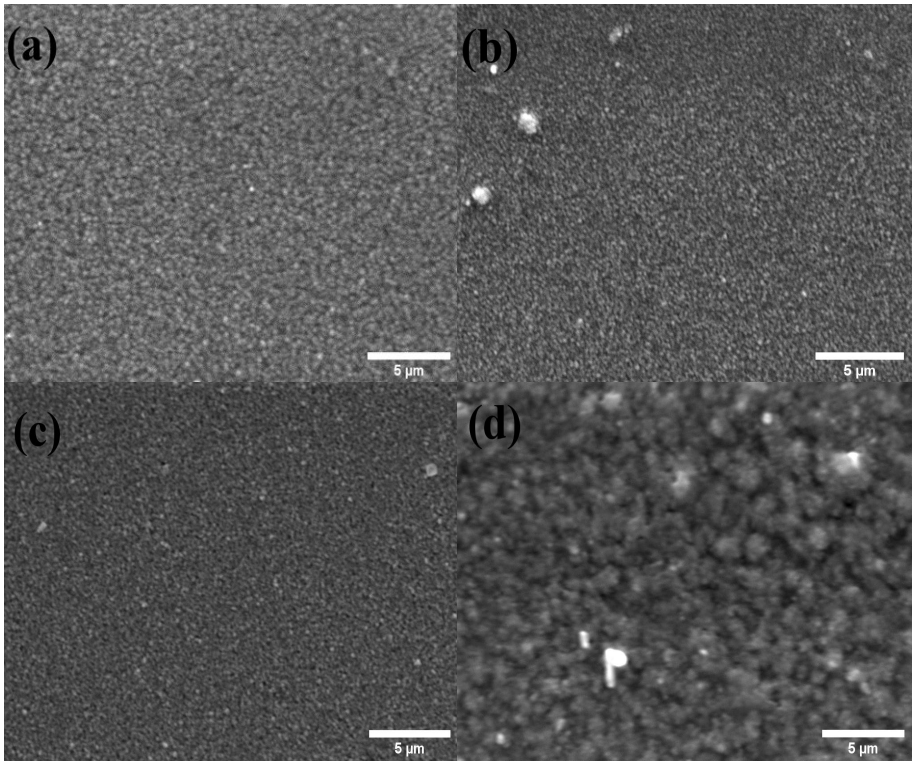

Fig. 2. SEM images of a) 5%Co-SnO_2, b)5%Cu-SnO_2, c) pure SnO_2 , and d)Fe-SnO_2 thin films, respectively.

3.3. Compositional analysis

The structural characterization of materials allows us to identify the phases present in them and to determine their chemical composition. The chemical composition allows us to know exactly the percentage of elements in our films.

EDAX spectra made on films of (a) SnO_2, (b) 5%Fe- SnO_2, (c) 5%Co- SnO_2 and (d) 5%Cu-SnO_2 are shown in the figure (Fig. 3a). The results show the presence of typical peaks on the spectra characterizing the elements Sn, O, Fe, Co and Cu. The presence of peaks related to foreign elements such as Si is due to the composition of the glass substrate used for the deposits. This varies from sample to sample due to the variation in the thickness of the doped layers [21].

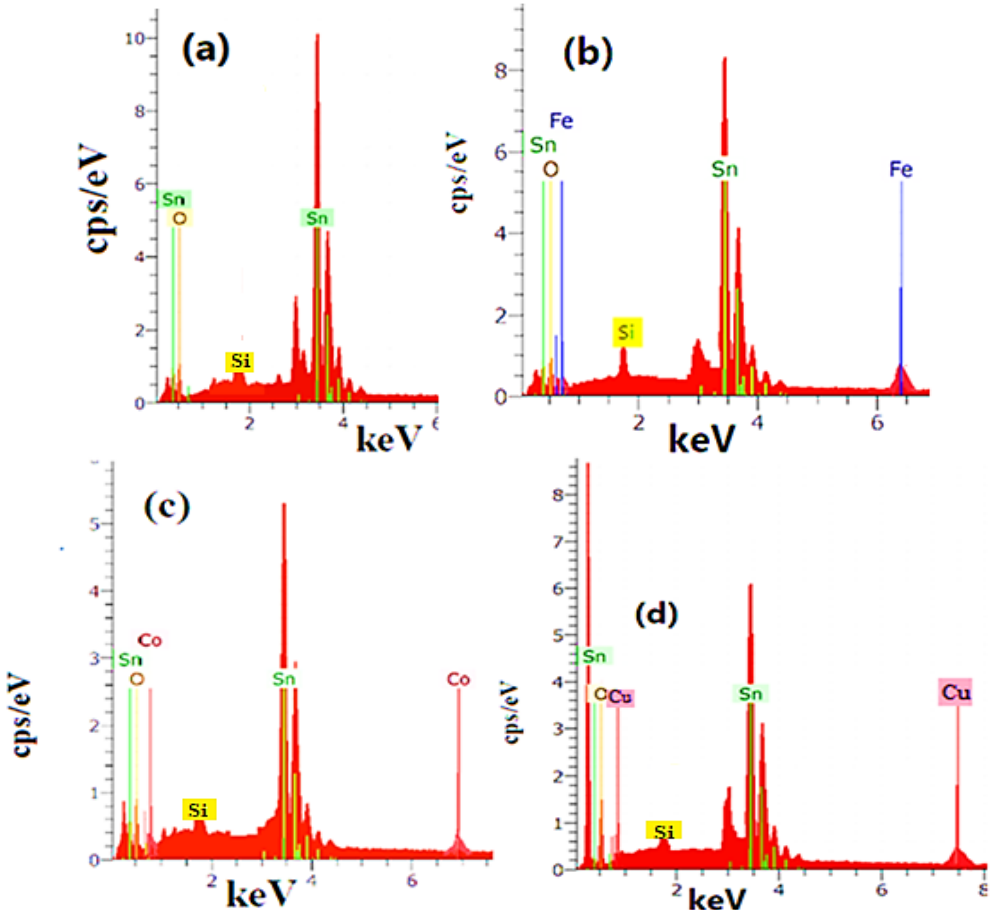

Fig. 3. EDAX elemental composition analysis of SnO_2 (a), SnO_2:Fe 5% (b), SnO_2:Co 5% (c) and SnO_2:Cu5% (d) thin films.

We evaluate the stoichiometry of the films exclusively from the M and Sn signals. We then take films of the stoichiometric form $Sn_{1-x}M_xO$ [5% -M = Fe, Co and Cu]. According the formula (Eq. (4)) [21,26]:

$$x = r/(1 + r), \tag{5}$$

With x as the atomic content of M, and r as the ratio between Sn and the EDAX signals of Sn and M (see Table 2). The results reveal The strong incorporation of transition elements in the structure. Fig. 4, which shows a ratio between the EDAX signals and the calculated atomic content of M, showing good effectiveness of the dopant elements (Fe, Co and Cu).

Table 2. Composition and stoichiometry of the pure and 5%-(Co, Fe, Cu)-doped SnO2 thin films obtained by statistical analysis of EDS spectra.

$Sn_{0.95}M_{0.05}O_2$ [M=Fe, Co, and Cu] ''Nominal'' M content (at.)	Sn (at.%)	O (at.%)	Fe (at.%)	Co(at.%)	Cu (at.%)	x (M) "EDS" M content (at)
SnO_2	82.68	17.32	-	-	-	-
$Sn_{0.95}Fe_{0.05}O_2$	75.52	20.12	4.36	-	-	0.0545
$Sn_{0.95}Co_{0.05}O_2$	78.49	16.83	-	-	4.68	0.0562
$Sn_{0.95}Cu_{0.05}O_2$	72.52	23.40	-	-	4.08	0.0532

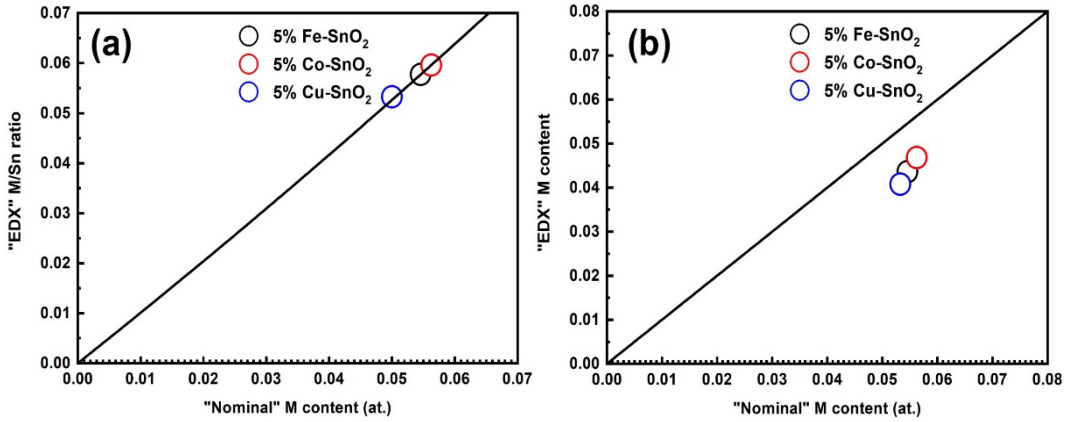

Fig. 4. a) M/Sn atomic ratio and b) M atomic content (measured with EDAX) plotted as function of the expected M content.

3.4. Fourier transform infrared (FTIR) analysis

Figure 5 represents the infrared spectra in absorption mode obtained respectively from $Sn_{0.95}M_{0.05}O_2$ [M = Co, Fe and Cu] thin films recorded between 400cm^{-1} and 4000cm^{-1} at room temperature.

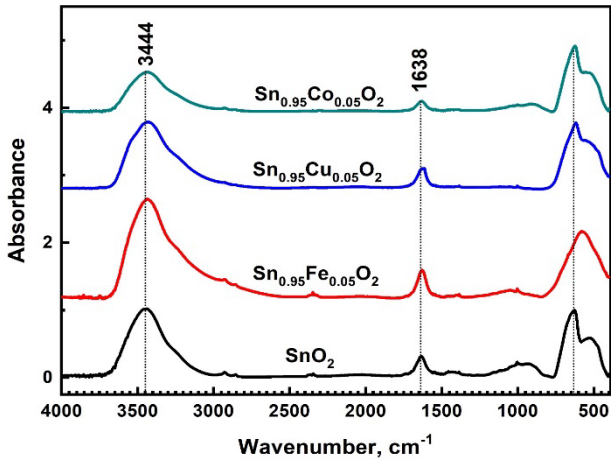

Fig. 5. FTIR spectra of the SnO_2, $Sn_{0.95}M_{0.05}O_2$ [M = Fe, Co, and Cu] samples.

The bands located at 3444 cm^{-1}, 1638 cm^{-1}, 1020 cm^{-1}, 1394 cm^{-1}, and 2346 cm^{-1} were observed due to the vibrations of hydrogen bonds in the adsorbed water molecules and the alcohol involved in the O-H oscillators, respectively [30]. The vibrations appearing at 2851 cm^{-1} and 2929 cm^{-1} correspond to vibrational modes of H_5O^{2+} ions [30], which are due to ethanol (C_2H_5- OH), these vibrations are more intense in the case of annealed samples. The bands appearing around 524 cm^{-1} and 640 cm^{-1} are typical for SnO_2 and are attributed to the absorption of the Sn-O-Sn bond and Sn-O bond vibrations in SnO_2 [30-33]. A positional shift for doped films, changes the shape of the characteristic vibration line (Sn-O) due to the deference of ionic radiation between Co^{2+} and Cu^{2+} ions [34]. For Fe-SnO_2 films, the band appearing around 579cm^{-1} corresponds to the O-Sn-O vibration, which confirms the substitution of Fe^{2+} in the SnO_2 network. Indeed, the ionic radius of Fe^{2+} (0.78 Å) being very close to that of Sn^{4+} (0.69 Å) but much smaller than that of O^{2-} (1.4 Å), the Fe ions occupy more easily the Sn sites of SnO_2.

3.5. Optical properties

The optical transmission spectra of the undoped SnO_2 and $Sn_{0.95}M_{0.05}O_2$ [M=Fe, Co and Cu] thin films are presented in Figure 6 which shows that all thin films have two regions: The first region at a wavelength above 400 nm shows practically the average transmission between 73-80% and reveals a variation of (T%) in nature of dopants and as a function of the calculated film thickness (t). It is found that the transparency depends on the thickness of the samples exposed in the Beer-Lambert law as shown in Table 3. It is noted that the transmittance is improved with the doping of copper and cobalt.

Table 3. Dispersion parameters of the 5%-(Co, Fe, Cu)-SnO_2 films extracted by fitting the experimental data.

Samples	**Transmittance** T%	**Thickness (nm)**	**Eg (eV)**	**n at 598 nm**	**n_∞**
SnO_2	73	700	3.75	1.83	1.78
5%Co_ SnO_2	76	651	3.87	1.76	1.72
5%Fe_ SnO_2	74	400	3. 96	1.74	1.70
5%Cu_ SnO_2	80	500	3.89	1.75	1.71

A region of strong absorption (λ< 400nm) in all films, this region corresponds to the fundamental absorption (. It is due to the interband electronic transition. The variation of the transmission in this region is exploited for the determination of the bandgap energy. The bandgap width (Eg) of SnO_2 and $Sn_{0.95}M_{0.05}O_2$ [M=Fe, Co and Cu] thin films was calculated by a single-effect oscillator fit suggested by Wemple et al [21- 26, 19]. In Figure 6, the solid curves indicate the curve fit while the symbols represent the data from the experiments. Table 4 shows the value of the products obtained.

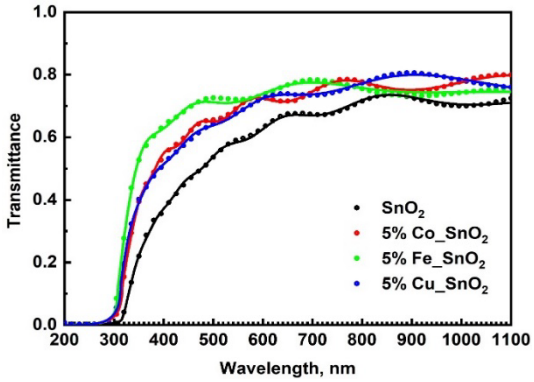

Fig. 6. Transmission spectra of SnO_2, $Sn_{0.95}M_{0.05}O_2$ [M = Co, Cu, and Fe]. Measured (full circles) and calculated (solid lines) transmittance spectra of films.

Table 4. Electrical properties of the undoped and 5%-(Co, Fe, Cu)-SnO_2 films.

Samples	**S, μV/K**	**n, cm^{-3}**	**E_F,meV**	**Thickness, nm**	**ρ, Ω. cm**	**σ, $Ω^{-1}. cm^{-1}$**
SnO_2	-76	1.9×10^{19}	96	700	1.8×10^{-2}	54.9
5%Co_ SnO_2	-110	9.8×10^{18}	66	651	1.4×10^{-2}	69.8
5%Fe_ SnO_2	-71	6.1×10^{19}	103	400	2.4×10^{-2}	41.6
5%Cu_ SnO_2	-133	6.6×10^{18}	55	500	4.2×10^{-2}	23.5

An increase of its energy level from 3.75 to 3.96 eV with the nature of the doping [M= Fe, Co and Cu] was noticed (Table 2). This development is due to the Burstein-Moss shift [35]. This result may be due to the defects created by the replacement of Sn^{4+} by Co_{2+}, Fe^{2+} and Cu^{2+} ions within the SnO2 structure, partly because of their electronegativity and the ionic radius between Sn4+ compared to the other doping ions. The energy shift (Eg) is proportional to the carrier concentration (Nv), which is consistent with the following electrical analyses. Indeed, these bandwidth values found during this work are consistent with those reported in publications [3, 36,37]. An increase in gap energy with the insertion of Co, Fe and Cu atoms as a dopant has been observed, this may be due to the presence of impurity concentration and disorder in the SnO_2 lattice, and/or could be a result of the increased grain size and shape effect [38,39].

The value of Eg is increased with the nature of Fe, Co, and Cu doping, which indicates some structural disorder related to the training of some defects and/or impurities causing localized states in the band structure. Therefore, the reduction in the bandgap energy as a function of the nature of the doping is due to the rise in disorder in the structure and density of the localized states.

The thickness of the thin films was estimated to be 400 nm to 700 nm, which is shown in Table 3. It can be seen that the thickest thickness is the undoped SnO_2 thin films. In addition, we know that the thickest thin films transmit little light. The undoped SnO_2 thin films has the lowest transmission value.

The calculated refractive indices [21-23, 26] of SnO_2 and $Sn_{0.95}M_{0.05}O_2$ [M=Fe, Co, and Cu] films are presented in Figure 7. It is interesting to note a decrease in the refractive indices of the films concerning the nature of the dopant. Indeed, the latter is influenced by structural defects (e.g., voids, dopants, inclusions). Consequently, this variation is probably related to the effect of the incorporation of (Fe, Co, and Cu) [21-23, 26], which results in an enhancement of the impurities in the carrier material.

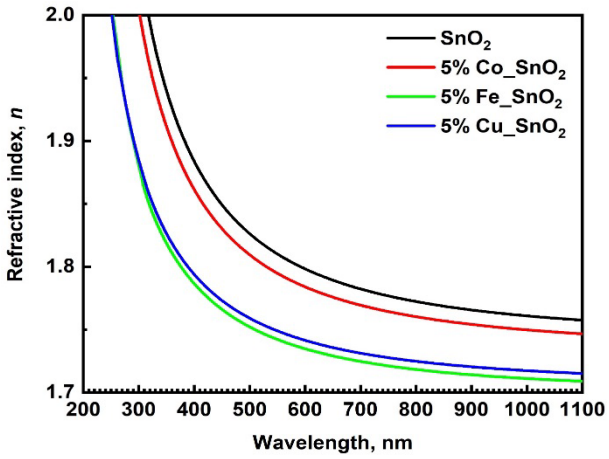

Fig. 7. Refractive index of SnO_2, $Sn_{0.95}M_{0.05}O_2$ [M = Co, Cu, and Fe] flms.

3.6. Electrical properties

To examine the influence of doping nature (Fe, Co, and Cu) on the electrical characteristics of SnO_2 thin films, the latter were investigated by measuring the Seebeck coefficient from 0 to 200K, electrical resistivity (ρ), carrier concentrations (n), and conductivity (σ).

Figure 8 shows the Seebeck coefficient (S) for undoped and 5% doped (Fe, Co and Cu) SnO_2 thin films.

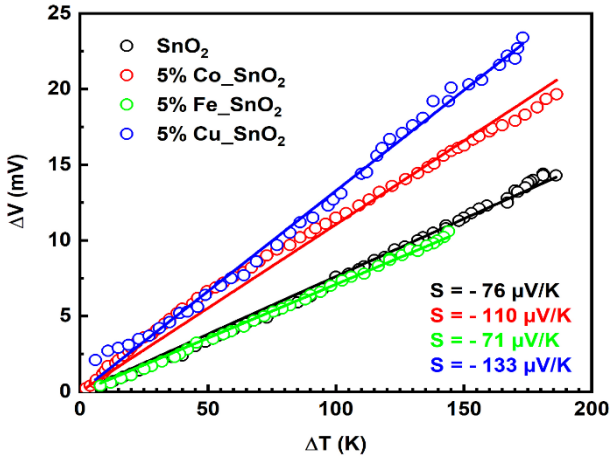

Fig. 8. Seebeck coefficients for SnO_2, $Sn_{0.95}M_{0.05}O_2$ [M = Co, Cu, and Fe] thin films.

It can be seen that the Seebeck coefficient is negative for all samples, thus verifying an n-type electrical conductivity. The Seebeck coefficient values are in the interval of S = -76µV/K, S = -110µV/K, and S = -71µV/K, and S= -133µV/K for SnO_2, 5%Co-SnO_2, 5%Fe-SnO_2, and 5%Cu-SnO_2 thin films respectively. The carrier concentration can be determined using the following equations [40]: when, $|S| > 75$ µV/K

$$m_S^* = \frac{h^2}{2k_BT}\left\{\frac{3n}{16\sqrt{\pi}}\left(exp\left[\frac{|S|}{\left(k_B/e\right)} - 2\right] - 0.17\right)\right\}^{2/3} \quad (6)$$

and, when $|S| < 75$ µV/K

$$m_S^* = \frac{3h^2}{8\pi^2 k_B T}\frac{|S|}{(k_B/e)}\left(\frac{3n_H}{\pi}\right)^{2/3} \quad (7)$$

where (mS_{SnO2}*(m^*_S= 0.216m_0) the effective mass, e is the charge of the carrier, k_B corresponds to the Boltzmann constant, T represents the absolute temperature, h is the Plank constant, and n the concentration of charge carriers. It is found that the carrier concentration is initially affected by the nature of doping and decreases with Co and Cu doping of the order of 1018 cm^{-3}, the reduction in carrier concentration with Co^{2+} and Cu^{2+} doping may result from the segregation of electrically inactive Co and Cu atoms in the grain boundaries and the incorporation of Co^{2+} and Cu^{2+} ions into the Sn lattice sites. For doping with Fe^{2+} ions, there is an increase in the carrier due to the institution of extra electrons.

The degenerate character of our SnO_2, $Sn_{0.95}M_{0.05}O_2$ [M=Fe, Co, and Cu] thin films is verified by determining their Fermi energy levels (F_E) using this equation[41]:

$$E_F = \frac{\pi^2 k_B^2 T}{3|e||S|} \quad (8)$$

The Fermi energy values is between 55 and 103 meV (Figure.9). It can be seen that the Fermi energy level (E_F) rises with Fe doping. Indeed, the extra electrons fill states in the conduction band, and the Fermi level is shifted to higher energy in the conduction band. On the other hand, all levels under the Fermi band are filled states, and therefore it is impossible to move the electron from the upper level of the valence band to the conduction band situated above the Fermi level. Due to the Pauli exclusion principle, excitation in these occupied states is impossible. As a consequence, an increase in the energy gap is detected. The detected red and/or blue shift shows an insignificant increase in the band structure of Fe-doped SnO_2 nanocrystalline films due to the integration of Fe^{2+}

ions. While the Fermi energy (F_E) level decreases with the doping of Co^{2+} and Cu^{2+} ions, this decrease reduces the Fermi level towards the center.

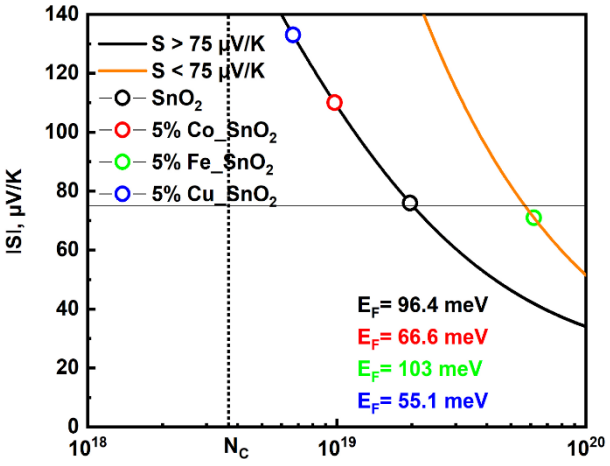

Fig 9. Seebeck coefficients as a function of carrier concentrations for SnO_2, $Sn_{0.95}M_{0.05}O_2$ [M = Co, Cu, and Fe] thin films.

These findings can be confirmed by calculating the values of the effective density in the conduction band, using the formula [42] that interpolates the interval between non-degenerate and degenerate semiconductors.

$$N_C = 2\left(\frac{2\pi m_S^* k_B T}{h^2}\right)^{3/2} \quad (9)$$

The value of the resulting effective density of SnO_2 is 3. 63×10^{18} cm-³. Figure 9 shows the degeneracy of the SnO_2, and 5%M (Fe, Co, and Cu) thin films. We noted that the thin films of $Sn_{0.95}Fe_{0.05}O_2$ highly degenerate which indicates that this element promotes electron formation, which confirms the substitution of iron in the SnO_2 host lattice. However, for the case of doping with the elements cobalt and coppper is less degenerated than SnO_2 which indicates that these elements do not promote electron formation which confirms that these elements entered the SnO_2 lattice as impurities.

Resistivity for the films decreases from 1.82 x 10^{-2} to 1.43 x 10^{-2} Ω. cm with cobalt doping. And increases by 2.4 x 10^{-2}, and 4.2 x 10^{-2} Ω. cm, for Fe, and Cu doping. For the conductivity (σ), the values vary with the nature of the dopant, and the thickness of the thin films. The results are presented in Table.4.

3.7. Photocatalytic performance of SnO2 and 5%-MSnO₂[M=Fe, Cu and Co] thin films

Fig.10. displays the changes of MB concentration with increasing irradiation time using SnO_2 and 5%-$MSnO_2$ [M=Fe, Cu and Co] thin films as photocatalysts. In all samples, they reveal the same trend, i.e. the MB concentration gradually decreases with increasing irradiation time. Under irradiation, SnO_2 absorbs photons and generates electrons and holes. If these electrons and holes can move to the surface of SnO_2 grains, they react with water and produce hydroxyl radicals [43, 44]. The hydroxyl radical is a powerful oxidizing agent that can degrade organic pollutants. Fig. 10 shows that Fe, Co and Cu doping improves the photocatalytic performance of SnO_2 thin films and accelerates the photo degradation reaction process.

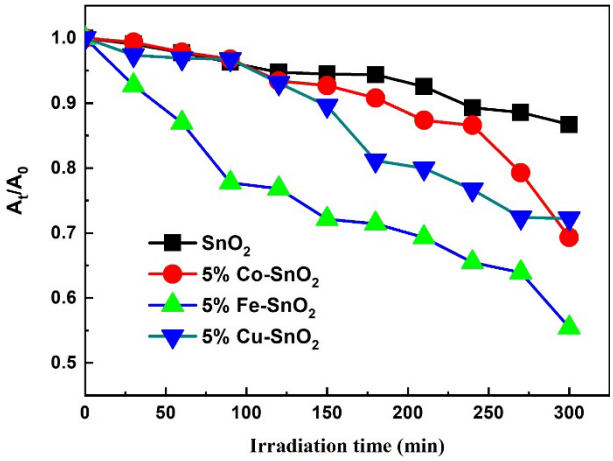

Fig. 10. MB concentration changes with irradiation time.

Fig. 11. shows the degradation rate (%) of the samples under irradiation for 5 h. For the first 120min the undoped, Co and Cu-doped SnO_2 thin films have the same degradation rate (≈5%), and the 5%Fe-SnO_2 thin films have a degradation rate of 23%. But after this time, compared to undoped SnO_2 thin films, the degradation efficiency of Cu, Co, Fe doped SnO_2 thin films is improved, especially for 5%Fe_SnO_2 samples (45%). As for the Co_SnO_2 (38%) and 5%Cu_SnO_2 (28%) and SnO_2 (15%) samples, the improvement of the photodegradation efficiency should result mainly from the reduction of the recombination of photogenic electrons and holes.

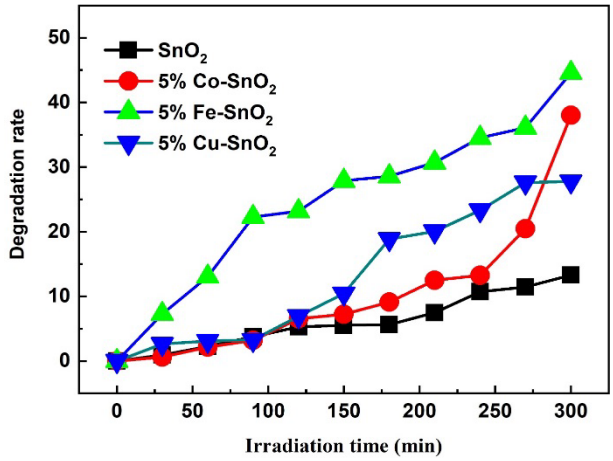

Fig. 11. The degradation rate (%) of the samples under UV irradiation.

The kinetics of the degradation reaction of MB in solution is shown in Fig. 12, and the calculated kinetic parameters of MB degradation are listed in Table 5, conforming with equation (10) [45].

$$A = X * \exp(-k * t) + E \tag{10}$$

where the unit of the (pseudo) rate constant of order k is the opposite unit of time used (min-1), and X is the process amplitude, E is the termination point, and both have identical units to the measured quantity A.

Table 5. Pseudo-frst-order kinetic parameters of MB degradation.

Samples	Value			Standard deviation			R^2
	K(min^{-1})	X	E	K(min^{-1})	X	E	
SnO_2	0.000051	13.701	-12.062	0.00149	393.405	393.41	0.9660
5% Fe_SnO_2	0.004473	0.8491	0.7296	0.00146	0.13967	0.1534	0.9703
5% Cu _SnO_2	0.000117	16.0557	-14.385	0.00572	771.027	771.09	0.6586
5% Co_SnO_2	0.003759	0.18090	1.0760	2066.99	0.13585	0.0429	0.1659

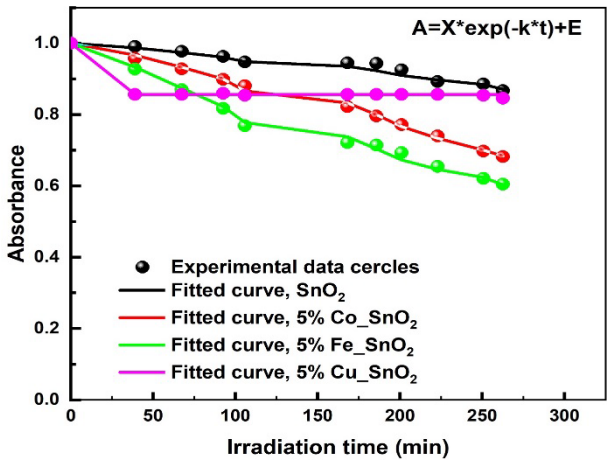

Fig. 12. Degradation kinetics of MB aqueous solutions by SnO_2, $Sn_{0.95}M_{0.05}O_2$ [M = Co, Cu, and Fe] without UV irradiation.

It is found that the dye degradation process proceeds optimally according to a pseudo-kinetic of order 1. The values of k for the thin films were SnO_2 (0.000051min^{-1}), 5%Fe_ SnO_2 (0.004473 min^{-1}), 5%Cu_ SnO_2 (0.000117 min^{-1}). 5%Co_ SnO_2 (0.003759min^{-1}). It can be noticed that doping with iron had the highest value of k than cobalt, and the doping with copper have the lowest value compared to undoped tin oxide films.

4. Conclusion

Successful deposition of pure and 5%-(Co, Fe, Cu) SnO_2 thin films on glass substrates by the spray pyrolysis technique is presented. The influence of the diversity of dopants (Co, Fe, and Cu) on the structural, optical, electrical, and photocatalytic properties of SnO_2 thin films had been analyzed. According to the x-ray diffraction pattern, it was found that the deposited films have a polycrystalline tetragonal rutile structure. Mesh lattice parameters and microstructure decreased with the insertion of the dopant transition metal. While SnO_2 thin films appeared more consistent in grain size and surface uniformity with the introduction of (Co, Fe and Cu). From the optical investigation, it was found that the films were dependent on the nature of the dopant and that (Co, Fe, Cu) doping favored the increase of the estimated band gap value. On the other hand, the Seebeck coefficient varied with the type of doping. Similarly, the charge concentrations are also impacted by the nature of the doping.

The resistivity was influenced by the nature of the doping, implying that Co-doped SnO_2 thin films are appropriate for use in optoelectronic components. For the photocatalytic tests, the best performance was observed for the $Sn_{0.95}Fe_{0.05}O_2$ samples of approximately (45%).

Acknowledgments

Funding was provided by the General Direction of research and development technologies/ Ministry of Higher Education and Research Sciences DGRSDT/ MESRS, Algeria. The financial support from Abbes Laghrour University of Khenchela (Algeria). The authors would like to thank the Project Research (PRFU) and LASPI^{2}A Laboratory of Khenchela University (Algeria) for their financial support of this research project.

References

[1] Roguai S and Djelloul A 2022 Bull. Mater. Sci. 45 227 ; https://doi.org/10.1007/s12034-022-02804-3

[2] Ikhmayies S J 2016 Int. J. Hydrogen Energ. xxx 1.

[3] Soitah T N, Yang C and Sun L 2010 Mat. Sci. Semicon. Proc. 13 125 ; https://doi.org/10.1016/j.mssp.2010.03.002

[4] Miao D, Zhao Q, Wu Sh, Wang Zh, Zhang X and Zhao X 2010 J. Non-Cryst. Solids, 356 2557 ; https://doi.org/10.1016/j.jnoncrysol.2010.06.076

[5] Batzill M, Katsiev K, Burst J M, Diebold U, Chaka A M and Delley B 2005 Phys. Rev. B72(165414) 1.

[6] Baden A D, Cox P A, Egdell R G, Orchard A F and Willmer R G D 1981 J. Phys. C: Solid State Phys. 14 L1081 ; https://doi.org/10.1088/0022-3719/14/34/003

[7] Diallo A, Manikandan E, Rajendran V and Maaza M 2016 J. Alloys Compd. 681 561 ; https://doi.org/10.1016/j.jallcom.2016.04.200

[8] Kaur J, Shah J, Kotnala R K and Verma K C 2012 Ceram. Int 38 5563 ; https://doi.org/10.1016/j.ceramint.2012.03.075

[9] Li G, Fang X, Feng W and Liu J 2017 J. Alloys Compd 716 106 ; https://doi.org/10.1016/j.jallcom.2017.04.288

[10] Mehraj S, Ansari M S and Alimuddin 2015 Physica E Low Dimens. Syst 65 84 ; https://doi.org/10.1016/j.physe.2014.08.016

[11] Li L, Yu K, Tang Z, Zhu Z and Wan Q 2010 J. Appl. Phys 107 014303 ; https://doi.org/10.1063/1.3273497

[12] Fitzgerald C B, Venkatesan M, Douvalis A P, Huber S, Coey J M D and Bakas T 2004 J. Appl. Phys 95 7390 ; https://doi.org/10.1063/1.1676026

[13] Wang H, Yan Y, Mohammed Y S, Du X, Li K and Jin H 2009 J. Magn. Magn. Mater. 321 3114 ; https://doi.org/10.1016/j.jmmm.2009.05.013

[14] Mishra R K, Kushwaha A and Sahay P P 2014 RSC Adv. 4 3904 ; https://doi.org/10.1039/C3RA43709D

[15] Soussia L, Garmim T, Karzazi O, Rmili A, El Bachiria A , Louardi A et al 2020 Surf. Interfaces 19 100467 ; https://doi.org/10.1016/j.surfin.2020.100467

[16] Preiß E M, Rogge T and Krauß A 2015 Procedia Eng 120 88 ; https://doi.org/10.1016/j.proeng.2015.08.572

[17] Shokr E Kh, Wakkad M M, Abd El-Ghanny H A and Ali H M 2000 J Phys Chem Solids . 61 75 ; https://doi.org/10.1016/S0022-3697(99)00234-6

[18] Dang H P, Ho Luc Q, Hieu Le V and Le T 2016 J. Alloys Compd 687 1012 ; https://doi.org/10.1016/j.jallcom.2016.06.236

[19] Arularasu M V, Anbarasu M, Pooveragan S, Sundaram R, Kanimozhi K and Maaza M 2018 J. Nanotechnol. 18 3511 ; https://doi.org/10.1166/jnn.2018.14658

[20] Kim G W, Sung C H, Anwar M S, Seo Y J, Heo S N, Park K Y et al 2012Curr. Appl. Phys. 12 S21 ; https://doi.org/10.1016/j.cap.2012.05.041

[21] Roguai S and Djelloul A 2020 Appl. Phys. A. 126 122 ; https://doi.org/10.1007/s00339-020-3301-6

[22] Roguai S and Djelloul A, Nouveau C, Souier T, Dakhel A A, Bououdina M 2014 J. Alloys Compd. 599 150 ; https://doi.org/10.1016/j.jallcom.2014.02.080
[23] Roguai S and Djelloul A 2019 Appl. Phys. A. 125 816 ; https://doi.org/10.1007/s00339-019-3118-3
[24] Amer M I, Moustafa S H and El-Hagary M 2020 Mater. Chem. Phys. 248 122892 ; https://doi.org/10.1016/j.matchemphys.2020.122892
[25] Ghosh S, Mandal M and Mandal K 2011 J. Magn. Magn. Mater. 323 1083 ; https://doi.org/10.1016/j.jmmm.2010.12.018
[26] Roguai S and Djelloul A 2021 Solid State Commun. 334-335 114362 ; https://doi.org/10.1016/j.ssc.2021.114362
[27] Benhaoua A, Rahal A, Benhaoua B and Jalaci M 2014 Superlattice Microst. 70 61 ; https://doi.org/10.1016/j.spmi.2014.02.005
[28] Anandhi R, Mohan R, Swaminathan K and Ravichandran K 2012 Superlattice. Microst. 51 680 ; https://doi.org/10.1016/j.spmi.2012.02.006
[29] Mariappan R, Ponnuswamy V, Ragavendar M, Krishnamoorthi D and Sankar C 2012 Optik-Int. J. Light Electron. Opt 123 1098 ; https://doi.org/10.1016/j.ijleo.2011.07.038
[30] Pereira M S, Lima F A S, Silva C B, Freire P T C and Vasconcelos I F 2017 J Sol-Gel Sci Technol 84 206 ; https://doi.org/10.1007/s10971-017-4488-7
[31] Siva Jahnaviv V, Kumar Tripathy S and Ramalingesw Aara Rao A V N 2019 Phys. B: Condens. Matter 565 61 ; https://doi.org/10.1016/j.physb.2019.04.020
[32] Velásquez C, Rojas F, Ojeda M L, Ortiz A and Campero A 2005 Nanotechnology 161278.
[33] Amalric-Popescu D and Bozon-VerdurazF 2001 Catal. Today 70 139 ; https://doi.org/10.1016/S0920-5861(01)00414-X
[34] Ghosh C K, Malkhandi S, Mitra M K and Chattopadhyay K K 2008 J. Phyis. D: App. Phys 41 245113 ; https://doi.org/10.1088/0022-3727/41/24/245113
[35] Park S M, Ikegami T, Ebihara K and Shin P K 2006 Appl. Surf. Sci. 253 1522 ; https://doi.org/10.1016/j.apsusc.2006.02.046
[36] Khelifi C, Attaf A, Saidi H, Yahia A, Dahnoun M and Saadi A 2016 Optik 127 11055 ; https://doi.org/10.1016/j.ijleo.2016.09.060
[37] Parthibavarman M, Renganathan B and Sastikumar D 2013 Curr. Appl. Phys. 13 1537 ; https://doi.org/10.1016/j.cap.2013.05.016
[38] Ngom B D, Mpahane T, Manikandan E and Maaza M 2016 J Alloys Compd 656 758 ; https://doi.org/10.1016/j.jallcom.2015.09.230
[39] Maaza M, Ngom B D, Achouri M and Manikadan K 2015 Vacuum 114 172 ; https://doi.org/10.1016/j.vacuum.2014.12.023
[40] Zevalkink A, Smiadak D M, Blackburn J, Ferguson A J, Chabinyc M L, Delaire O et al 2018 Appl. Phys. Rev. 5 021303 ; https://doi.org/10.1063/1.5021094
[41] MacDonald D K C 1962 Thermoelectricity: an introduction to the principles (Wiley, New York, London).
[42] Boy J, Handwerg M, Ahrling R, Mitdank R, Wagner G, Galazka Z et al 2019APL Mater. 7 022526 ; https://doi.org/10.1063/1.5084791
[43] Jusoh N W C, Jalil A A, Triwahyono S, Karim A H, Salleh N F, Annuar N H R et al 2015 Appl. Surf. Sci. 330 10 ; https://doi.org/10.1016/j.apsusc.2014.12.192
[44] Jayaraman V K, Hernández-Gordillo Aand Bizarro M 2018 Mater. Sci. Semicond. Process.75 36 ; https://doi.org/10.1016/j.mssp.2017.11.015
[45] Lente G (2015) Deterministic kinetics in chemistry and systems biology. Springer, New York, pp 52-58 ; https://doi.org/10.1007/978-3-319-15482-4